Arabian Journal of Chemistry (2019) 12, 3678–3691

King Saud University

Arabian Journal of Chemistry

www.ksu.edu.sa
www.sciencedirect.com

ORIGINAL ARTICLE

The nature and kinetics of the adsorption of dibenzothiophene in model diesel fuel on carbonaceous materials loaded with aluminum oxide particles

Mazen K. Nazal [a,b,*], Mazen Khaled [a,*], Muataz A. Atieh [c], Isam H. Aljundi [d,e], Ghassan A. Oweimreen [a], Abdalla M. Abulkibash [a]

[a] *Chemistry Department, King Fahd University of Petroleum & Minerals (KFUPM), Saudi Arabia*
[b] *Center for Integrative Petroleum Research (CIPR), Research Institute (RI), KFUPM, Saudi Arabia*
[c] *Qatar Environment and Energy Research Institute, Qatar Foundation, PO Box 5825, Doha, Qatar*
[d] *Chemical Engineering Department, King Fahd University of Petroleum & Minerals (KFUPM), Saudi Arabia*
[e] *Center of Excellent in Nanotechnology (CENT), Research Institute (RI), KFUPM, Saudi Arabia*

Received 1 September 2015; accepted 2 December 2015
Available online 15 December 2015

KEYWORDS

Selectivity;
Adsorptive desulfurization;
Adsorption isotherms;
Thiophenic compounds;
Model fuel

Abstract The resulted environmental and industrial problems from presence of sulfur compounds such as dibenzothiophene (DBT) in some fuel led to attract greater interest in research on the removal of these compounds. In this study the adsorption isotherms of dibenzothiophene (DBT) in model diesel fuel were obtained and desulfurization kinetics was carried out. The adsorbents used were commercial coconut activated carbon (AC), multiwall carbon nanotubes (CNT) and synthesized graphene oxide (GO) loaded with 5% and 10.9% aluminum (Al) in the form of aluminum oxide (Al_2O_3) particles to improve the chemical properties of their surface. The physicochemical properties for these adsorbents were characterized using thermal gravimetric analysis (TGA), N_2 adsorption–desorption surface area analyzer, scanning electron microscope (SEM), energetic dispersive X-ray diffractogram (EDX), field emission electron microscope (FE-TEM) and X-ray photoelectron spectrometer (XPS). The adsorption capacities for DBT on the aluminum oxide modified adsorbents are improved by about twofold, which is attributable to introduction of Al_2O_3 Lewis acid as an additional adsorption site. The highest adsorption capacity for DBT (85 ± 1 mg/g) with high selectivity factor relative to naphthalene (54 mg/g) was achieved using loaded activated carbon

* Corresponding authors at: King Fahd University of Petroleum & Minerals (KFUPM), Dhahran 31261, Saudi Arabia. Tel.: +966 13 860 8316 (M.K. Nazal).
E-mail addresses: mazennazal@kfupm.edu.sa, mazen_nazzal1981@hotmail.com (M.K. Nazal), mkhaled@kfupm.edu.sa (M. Khaled).
Peer review under responsibility of King Saud University.

Production and hosting by Elsevier

http://dx.doi.org/10.1016/j.arabjc.2015.12.003

with 5% Al. The adsorption capacities, removal selectivity and efficiencies with which the other prepared adsorbents remove DBT from model fuel are reported. The adsorption isotherms fitted both the Langmuir and Freundlich models. The adsorption rate for DBT follows pseudo-second order kinetics with correlation coefficients close to 1.00. The adsorbents are stable and reusable for at least 5 times.

1. Introduction

Severe environmental and industrial hazards result from the naturally occurring dibenzothiophene (DBT), and its derivatives, present in diesel fuel. These include catalytic poisoning, corrosion in pipes and emission of SO_x gases that contribute to acid rain (Kim et al., 2006). These hazards resulted in increasingly restrictive regulations on the contents of these compounds in diesel fuel. The European regulation lowered the specification for the sulfur content in diesel fuel from 2000 ppmw in 1991 to 50 ppmw in 2005 then to 10 ppmw in 2009 (Commission, 2009; Directive). By 2006 the U.S. Environmental Protection Agency (USEPA) restricted sulfur content to 15 ppmw and 30 ppmw in diesel and gasoline fuels respectively (Beardsley and Lindhjem, 1998; Bertelsen, 2001). Such restriction led to greater interest in research on the removal of sulfur compounds from fuels.

The removal of DBT and its derivatives is challenging in view of steric hindrance by their structures (Seredych et al., 2012; Tao et al., 2009). The conventional hydrodesulfurization (HDS) process used in the refining industries can bring the sulfur compound level to around 500 ppm; a value well above the requirements in the new regulations. To reach lower sulfur levels in the fuel using hydrodesulfurization, higher pressures and temperatures have to be used which make the process costly and lower the octane level of the fuel (Song and Ma, 2003). To obtain ultra clean diesel fuels chemical oxidation (Chamack et al., 2014; Cortes-Jácome et al., 2007; Zhu et al., 2007), photooxidation (Matsuzawa et al., 2002; Shiraishi et al., 1999; Tao et al., 2009) and adsorption (Liu et al., 2013; Seredych and Bandosz, 2009, 2010a,b, 2011; Srivastav and Srivastava, 2009; Yang et al., 2003) techniques were used.

The adsorption technique is promising as an alternative or complementary technique because it is simple, relatively cost effective and has the potential to remove the aromatic organic sulfur compounds from fuels to nearly zero level. Metal–organic frameworks derived carbon (Shi et al., 2014), Metal–organic frameworks composites (Hasan and Jhung, 2015), Zeolites (Yang et al., 2003), activated alumina (Kim et al., 2006; Srivastav and Srivastava, 2009), modified bentonite and montmorillonite clay (Ahmad et al., 2017; Ishaq et al., 2015) and different carbon materials such as activated carbon, graphite oxide, graphene and single wall carbon nanotube (Chen et al., 2004; Kumagai et al., 2010; Mabayoje et al., 2012; Seredych and Bandosz, 2009; Song et al., 2012; Wang et al., 2010; Yang et al., 2010) have been explored and used for removal of organic sulfur compounds from various model fuels and oil types.

Among the carbonaceous materials, the activated carbon with high surface area and high average pore volume is known as an excellent adsorbent for organic molecules such as DBT. Kim et al. (2006) found that at room temperature, the activated carbon is the best adsorbent among the raw activated alumina or alumina modified with Ni/SiO_2 for sulfur compounds. Kumagai et al. (2010) studied the adsorption behavior of DBT from *n*-hexane model diesel on coconut shell activated carbon and compared it with activated carbon fiber and found that, at low DBT concentration the adsorption capacity of activated carbon is higher than that of activated carbon fiber in spite of the fact that activated carbon fiber has higher surface area.

Graphite oxide has received high attention to be adopted for many applications due to their distinct properties. Possessing the graphite oxide oxygenated functional group makes it able to be modified with different metals oxide or other functional groups to improve its surface chemistry and anchoring additional active sites (Mabayoje et al., 2012). Graphene and graphene oxide based materials are known to be useful for the removal of toxic gases and for water purification (Mabayoje et al., 2012; Yang et al., 2010). Hoon and co-workers (Song et al., 2012) studied the adsorption of DBT on graphene and graphite oxide adsorbents prepared with phosphoric acid and compared their adsorption capacity with graphene and graphite oxide prepared by the conventional Hummers's method and reported that, graphite oxide and graphene which are prepared using phosphoric acid have higher surface area and adsorption capacity for DBT. Wang et al. (2010) explored the potential use of single wall carbon nanotube (SWCNT) as a drug carrier and adsorbent for N and S-heterocyclic aromatic compounds including thiophene compound as a model S-heterocyclic aromatic compound. They found the O-functional group on the oxidized CNT could enhance the adsorption of these compounds based on two main enhancement adsorption mechanisms which are electron donor–acceptor interaction and Lewis acid–base interaction with the CNT.

The chemistry of adsorbents' surface is a crucial factor for DBT adsorption, whereas the acidic groups (Seredych et al., 2009) and metal oxides such as MgO, ZnO, Al_2O_3 and TiO_2 (Lucas et al., 2001) on the surface of adsorbent play a major role in improving their surface and in turn enhance adsorption of DBT. This chemistry is attributed to Bronsted acid and Lewis acid of varying coordination (Lucas et al., 2001). Selectivity and activity of metal oxides are related to their acid–base properties which are a function with constituents, preparation method, composition and pre-treatment conditions (Tanabe, 1981). Hydrogen bonding between the associated hydroxyl groups on the adsorbent's surface with the lone electron pair on sulfur atom and/or electron cloud on aromatic rings in structure of the sulfur compound can play a significant role in the adsorption of sulfur compounds (Gutiérrez-Alejandre et al., 2006).

The scientific and industrial societies are seeking continually alternatives to the present adsorbents with new ones that have better properties such as, lower mass to volume ratio with high adsorption capacity. Modification of the carbonaceous nanomaterials such as CNT and GO which have distinct properties with a low cost and high thermal stability metal oxide such as aluminum oxide that has unsaturated surface can provide a strong electron acceptor site (Lewis acid) and hydroxyl group (Bronsted acid), as a result of improving the adsorption capacity for sulfur compounds. Therefore, this study investigates the potential use of CNT, GO and AC, loaded with both 5% and 10.9% aluminum in the form of the aluminum oxide as adsorbents for DBT. These percentages are denoted by the endings AL5 and AL10 in the notations ACAL5, ACAL10, CNTAL5, CNTAL10, GOAL5, and GOAL10. These adsorbents were characterized using thermal gravimetric analysis (TGA), an N_2 adsorption–desorption surface area analyzer, scanning electron microscopy (SEM), energetic dispersive X-ray diffractogram (EDX), field emission transmission electron microscope (FE-TEM) and X-ray photoelectron spectrometer (XPS), then the nature and kinetics of the adsorption of DBT from its solution in model diesel were studied. To decide on the best adsorption isotherm and the model for the adsorption kinetics the resulting data were fitted to equations for different adsorption isotherms. Additionally, the adsorbents' reusability and their selective adsorption of DBT relative to thiophene and naphthalene were studied.

2. Experimental

2.1. Materials

Multi-wall carbon nanotube (CNT) was purchased from Timesnano Company with purity 95%, outer diameter (OD) 10–20 nm, length 10–30 μm and a specific surface area (SSA) 200 m^2/g. The coconut activated carbon (AC) was purchased from Cenapro Chemical Corporation, Mandaue City, Philippine and they were used as received. Graphene oxide (GO) was prepared using Hummers's method described elsewhere (Hummers Jr and Offeman, 1958). Analytical grade ethanol, sulfuric acid, graphite powder >99%, potassium permanganate, hydrogen peroxide, hydrochloric acid, standard thiophene >99%, dibenzothiophene >99% and anhydrous HPLC grade *n*-hexane were obtained from Sigma–Aldrich. Naphthalene >98% was obtained from Fluka and 99.9% aluminum nitrate nonahydrate ($Al(NO_3)_3{\cdot}9H_2O$) was obtained from Research lab. The real diesel sample was purchased from a Sahel local gas station in Dhahran, Saudi Arabia. The DBT concentration in this sample was determined using gas chromatography (Agilent 7890 A) coupled with a sulfur chemiluminescence detector (GC-SCD) (Dual Plasma Technology 355) using hydrophobic Agilent DB-1 GC capillary column (30 m × 0.32 mm × 1 μm).

2.2. Adsorbents preparation and characterization

AC, CNT and GO were loaded with both 5% and 10.9% Al in the form of Al_2O_3 using the incipient wetness impregnation method. The resulting adsorbents are denoted by ACAL5, ACAL10, CNTAL5, CNTAL10, GOAL5, and GOAL10. Accurately weighed 15.3 g of $Al(NO_3)_3{\cdot}9H_2O$ dissolved in 400 mL ethanol contains 1% deionized water solution which was added slowly with stirring to 9.0 g of AC, CNT or GO to obtain carbon materials loaded with 10.9% Al (18.8% Al_2O_3). The resulting mixtures were homogenized using an ultrasonic vibrator (UP400S Hielscher-Ultrasound Technology) for 2 h to obtain a uniform loading of aluminum oxide on the surface of the carbon materials. Next they were dried in an oven (Precision from Thermo Scientific) at 80 °C for 48 h. The resulting solid materials were ground and calcinated in a furnace (Lindberg Blue M Thermo Scientific) at 350 °C for 2 h. The produced impregnated adsorbents were stored in tightly closed vials before using them in the experiments. In case of doping with 5.0% Al (9.0% Al_2O_3) the same procedure was followed by mixing 6.95 g $Al(NO_3)_3{\cdot}9H_2O$ with 9.5 g AC, CNT or GO. The thermal oxidation of raw and loaded AC, CNT and GO was investigated using TGA (TA Instrument Q Series Q600 SDT). The oxidation parameters were fixed at 10 mg of sample with heating rate of 10 °C/min and oxidation temperature from 25 to 800 °C under atmospheric air flow rate of 100 mL/min and their degradation under a nitrogen atmosphere flow rate of 100 mL/min. The adsorbents' textures and morphologies were studied using scanning electron microscope (SEM) (TESCAN LYRA3) coupled with Energy-dispersive X-ray spectroscopy (EDX) Oxford detector model X-Max. A JOEL-2100F Field Emission Transmission Electron Microscope (FE-TEM) was used for particle size measurement. The state of aluminum loaded on the adsorbents surface was determined using an X-ray photoelectron spectrometer (XPS) (Thermo Scientific ESCALAB 250Xi).

2.3. Adsorbents' surface pH measurements

A 0.20 g sample of the well dried adsorbent suspended in 10 mL distilled water underwent ultrasonic vibration for 2 h. The suspension was filtered and the pH of the filtrated solution was measured using a pH meter (Thermo Scientific CyberScan pH 1500).

2.4. Characterization of the adsorbents surface area and porosity

The surface area and porosity of the adsorbents were analyzed using 0.25 g samples in an automated gas sorption analyzer (Autosorb iQ Quantachrome USA) at relative pressures between 0.10 and 1.00. The liquid nitrogen adsorption–desorption isotherms were measured after degassing all the adsorbents at 200 °C to a pressure of 6.5×10^{-5} Torr. The Brunauer–Emmett–Teller (BET) (Dubinin, 1966) and the density functional theory (DFT) (Lastoskie et al., 1993) methods were used to calculate the surface area (SA) and total pore volume (V) respectively.

2.5. Analytical method

In the adsorption experiments, the thiophene, DBT and naphthalene concentrations were measured before and after the adsorption using HPLC-UV system (Agilent Technology 1260 Infinity series) and the chromatographic parameters are summarized in Table 1. Details of experimental procedures are shown in the supporting materials.

2.6. Adsorption experiments

The adsorption of DBT on pristine and impregnated AC, CNT and GO with 5 and 10.9 wt% Al in the form of Al_2O_3 was performed at 25 °C and shaking speed of 200 rpm using a batch mode experiment. For studying its adsorption isotherms,

Table 1 Chromatographic conditions used in the analysis.

Parameters	Description
Mobile phase	100% *n*-Hexane
Analytical column	Silica, 5 μm (200 × 4.6 mm i.d.)
Guard column	C18, 5 μm (10 × 4.6 mm i.d.)
Auto-sampler temperature	24 °C
Flow rate	1.0 mL/min
Back pressure	29–30 bar
Column temperature	24 °C
Injection volume	5 μL
Wavelength	In first 3.5 min the λ is 235 nm for thiophene and from 3.5 to 5.0 min the λ is 280 for DBT and naphthalene detection
Total run time	5.5 min

solutions of DBT at concentrations of 25, 50, 100, 125, 150, 200, and 250 mg/L in 25 mL *n*-hexane as a model fuel were each used with 150 mg of adsorbent and contact time for 2 h. To study its adsorption kinetics on the developed adsorbents, a 25 mL model fuel solution with an initial concentration of 250 mg/L DBT was added to 150 mg of the adsorbent in a vial that was capped then shaken continuously for a fixed time intervals. The adsorbent was then allowed to settle and quickly a 5 mL sample was removed and filtered. The same procedure was carried out for shaking time intervals of 10, 20, 30, 40, 60, 120, 240 and 1560 min. The effect of the adsorbent amount on the removal of DBT with initial concentration of 250 mg/L was studied by varying the adsorbent mass from 100 to 1500 mg. The removal efficiency was calculated using the following equation:

$$\text{Removal efficiency } \% = \frac{(C_o - C_e)}{C_o} \times 100\% \quad (1)$$

where C_o in mg/L is the initial concentration of the sulfur compound in the solution and C_e in mg/L is the equilibrium concentration of DBT sulfur compound in the solution.

2.7. Selectivity experiment

The selectivity of ACAL5 and CNTAL5 for DBT removal from a model fuel has been studied relative to thiophene as model molecule for small aromatic heterocyclic compounds, as well as relative to naphthalene which represents the availability of polyaromatic hydrocarbons (PAH) with molecular structures close to that of DBT. The stock solution for the ternary mixture from these three compounds thiophene/DBT/naphthalene in *n*-hexane was prepared with concentrations of 250 mg/L for both thiophene and DBT and 1000 mg/L for naphthalene to simulate the actual availability of PAH in real diesel. A 150 mg adsorbent was used in 25 mL of model diesel solution and the batch adsorption experiments were performed over a wide range of adsorbate concentrations at 200 rpm shaking speed and a 120 min adsorption time at room temperature. The concentrations of these three compounds were measured simultaneously before and after the adsorption equilibrium was achieved.

The distribution coefficient K_d (L/g) was calculated for each analyte based on the following equation:

$$K_d = \frac{q_e}{C_e} \quad (2)$$

where q_e is the adsorption capacity (mg/g) and C_e (mg/L) is the equilibrium concentration of one of the sulfur compounds or naphthalene. The distribution coefficient is used later to calculate the selectivity factor for DBT with respect to thiophene and naphthalene according to following equation:

$$k = \frac{K_{d(DBT)}}{K_{d(C)}} \quad (3)$$

where k expresses the adsorption selectivity factor using ACAL5 and CNTAL5, K_d is the distribution coefficient and the subscript (c) is the competing molecule (i.e. thiophene or naphthalene).

3. Results and discussion

3.1. Adsorbent characterization

3.1.1. Thermal gravimetric analysis

As shown in Fig. 1, the residual solvents evaporated below 100 °C while the initial oxidation temperature of raw AC, CNT and GO starts approximately at 400 °C, 550 °C and 500 °C respectively. However the final oxidation temperature for AC, CNT and GO was at 600 °C, 650 °C and 700 °C respectively. AC, CNT and GO loaded with 10.9% Al in the form of Al_2O_3 show the same results as raw carbon materials. The same experiment also shows that aluminum nitrate nonahydrate starts dehydrating at around 110 °C while the calcination temperature of aluminum nitrate starts at 200 °C and is complete at around 400 °C. Unmodified and modified GO with aluminum nitrate salt lost about 20% of their weight at around 200 °C. This may be explained by reduction of some of oxygenated groups present on the graphene surface and exfoliation graphene oxide sheets and releasing any trapped water molecules. The dehydration of aluminum nitrate nonahydrate and its conversion to aluminum oxide on different carbon materials was also confirmed under nitrogen gas which gave the same trend of results as under air as shown in Fig. 2.

3.1.2. Adsorbent texture and morphology

The SEM images of AC, CNT and GO are given before and after impregnation with Al_2O_3 particles in Fig. 3. A layer of Al_2O_3 particles covers the surface of the AC and GO sheets, while spherical particles cover the surface of the CNT. The difference in shape of Al_2O_3 particles may be attributed to the difference in the nature of AC, GO and CNT surfaces which in turn affect on the formation of Al_2O_3 particles. The elemental composition of the Al_2O_3-impregnated carbon based adsorbents was obtained by energy dispersive X-ray analysis (EDX) which is summarized in Table 2. It was found that the GO has higher oxygen content compared to AC and CNT due to the availability of oxygenated functional groups on the GO surface. In addition the oxygen percentage increased after impregnation with aluminum oxide particles and the percentages of aluminum in the adsorbents are close to the theoretical percentages (5% and 10.9%). TEM images for raw and loaded CNT and GO are shown in Fig. 4. The images show that all the nanotubes are hollow with many curvature sites, while the graphene oxide looks like multilayered wrinkled flakes. The TEM image in Fig. 4b shows the aluminum oxide nanoparticles dispersed on CNT were spherical with diameters between 30 and 80 nm. For loaded GO the nature of the aluminum oxide particles was difficult to predict so the diffraction pattern was obtained from the TEM for both GO and GO loaded with aluminum oxide to confirm that the GO layers were covered by Al_2O_3 after the impregnation as shown in Fig. 4d.

For further evidence the X-ray photoelectron spectrometer (XPS) (Thermo scientific ESCALAB 250Xi) was used to confirm the availability of aluminum oxide (Al_2O_3). The XPS survey spectrum in Fig. 5a shows the binding energies peaks in the range 284–290 eV match the values for C 1s in C—C, C═C, C—OH, C═O, C—OR, C—OOR and C—O—OH. Single element scan spectra in Fig. 5b and c show binding energies peaks at 532.8 and 534.5 eV which are attributed to the O 1s in

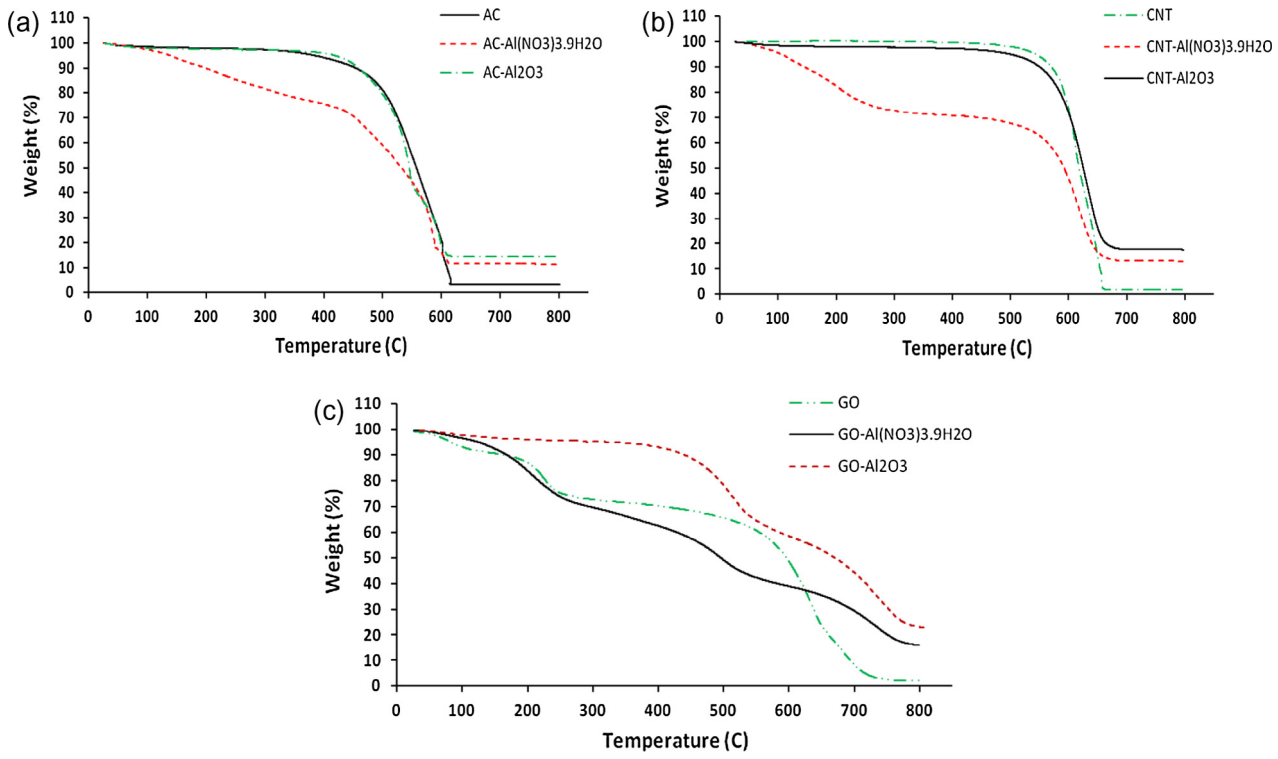

Figure 1 TGA under air atmosphere with a flow rate of 100 mL/min for (a) AC, (b) CNT and (c) GO impregnated with $Al(NO_3)_3{\cdot}9H_2O$.

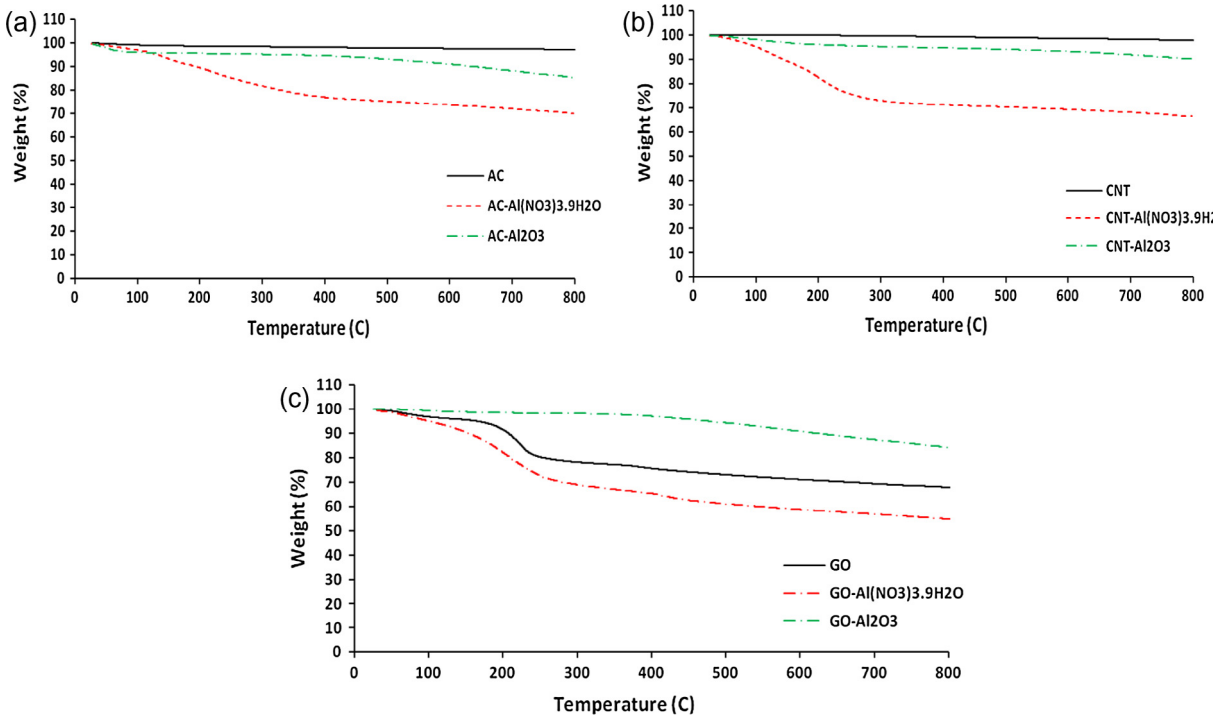

Figure 2 TGA under nitrogen atmosphere with a flow rate of 100 mL/min for (a) AC, (b) CNT and (c) GO impregnated with $Al(NO_3)_3{\cdot}9H_2O$.

physically adsorbed water molecules and the oxygenated functional group on the CNT, while the binding energies of 74.6 and 531.4 eV match the XPS fitting online library (NIST XPS, 2015) values for the Al 2p electron and the O 1s electron in Al_2O_3.

The surface area and porosity characterization results given in Table 3 show that for the pristine adsorbents the trend in surface area is AC > CNT > GO while the trend in total pore volume is CNT > AC > GO. Table 3 also shows that all impregnated adsorbents have lower surface areas, porosities

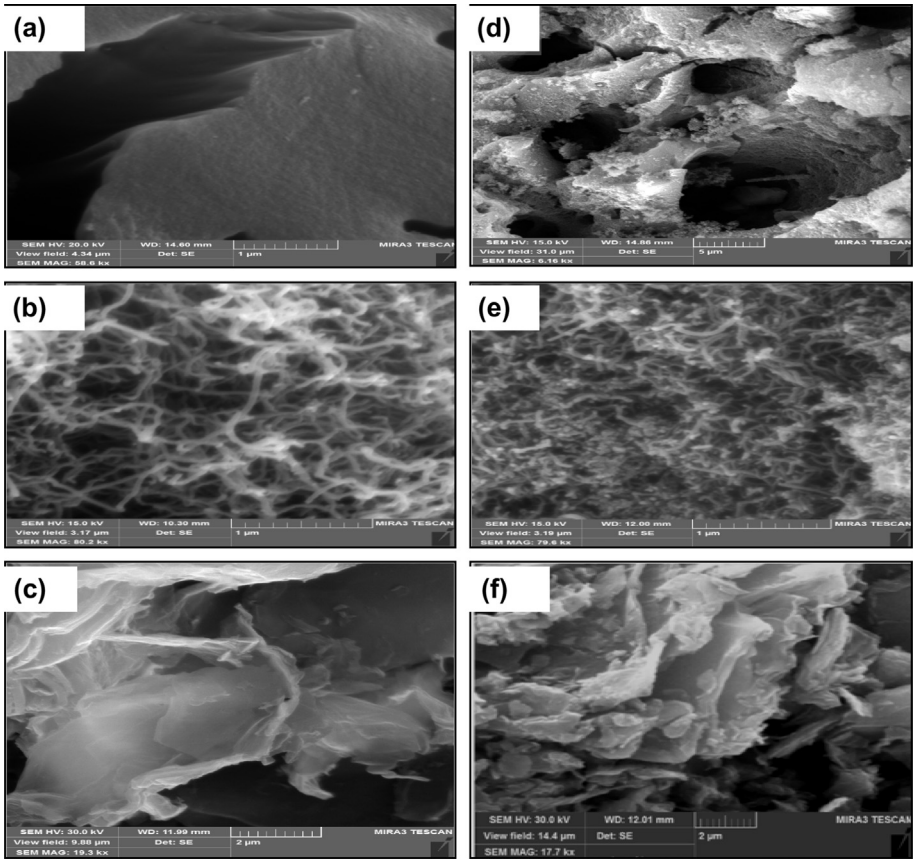

Figure 3 SEM images of (a) AC, (b) CNT and (c) GO before impregnation with Al_2O_3, (d) ACAL10, (e) CNTAL10 and (f) GOAL10.

and surface pH values relative to their corresponding pristine adsorbents. Both effects are accounted for by the accumulation of the amphoteric Al_2O_3 particles on the surfaces of the pristine adsorbents (Abu Safieh et al., 2015; Yu et al., 2005; Zhou et al., 2006).

3.2. Adsorption isotherms of dibenzothiophene

The respective Langmuir and Freundlich adsorption isotherms are presented respectively in Figs. 6 and 7 for DBT on ACAL5, ACAL10, CNTAL5, CNTAL10, GOAL5, and GOAL10. The Langmuir model assumes adsorption on a homogeneous adsorbent surface with identical adsorption sites and no interaction between molecules on neighboring sites. According to this model the adsorption capacity at equilibrium q_e is given by Eq. (4),

$$q_e = \frac{(Q_{max} b C_e)}{(1 + bC_e)} \tag{4}$$

where Q_{max} in mg/g is the maximum adsorption capacity, b is Langmuir constant and C_e in mg/L is the concentration of the sulfur compound in the solution at equilibrium. q_e is also given by Eq. (5),

$$q_e = \frac{V(C_o - C_e)}{(m)} \tag{5}$$

where V in mL is the volume of solution in the adsorption experiment, C_o in mg/L is the initial concentration of the sulfur compound in the solution and m in mg is the mass of adsorbent. Eq. (4) can be rearranged to the linear form as follows:

$$\frac{C_e}{q_e} = \frac{1}{bQ_{max}} + \frac{C_e}{Q_{max}} \tag{6}$$

The Freundlich model assumes that the adsorbent surface is heterogeneous with a multi-layer adsorption capacity (Adamson and Gast, 1967). According to this model,

$$q_e = K_F C_e^{1/n} \tag{7}$$

where K_F is the Freundlich constant and the parameter n is a measure of the heterogeneity of the surface of the adsorbent. The linear form of Eq. (7) is

$$\ln(q_e) = \ln(K_F) + \frac{1}{n}\ln(C_e) \tag{8}$$

The maximum adsorption capacity (Q_{max}) for each adsorbent was obtained from the slope of a linear least squares fit of C_e/q_e versus C_e (Eq. (6)). The n value for each adsorbent was obtained from the slope of a linear least square fit of $\ln(q_e)$ versus $\ln(C_e)$ (Eq. (8)) while the K_F value was calculated from its intercept. n and K_F give an idea about the degree of surface heterogeneity and the adsorption capacity respectively. Larger n and K_F values correspond respectively to greater heterogeneity on the adsorbent's surface and a higher adsorption capacity (Li et al., 2002). As shown in Table 4 for DBT there is no significant change in the n values of modified adsorbents. These n values fall between 1.2 and 1.9 which indicate DBT tendency for adsorption. While K_F increased for modified

Table 2 EDX results for carbon adsorbents before and after impregnation with Al_2O_3.

Adsorbent	Element	Weight%
AC	C	92.01
	O	7.99
ACAL10	C	62.11
	O	23.05
	Al	12.95
ACAL5	C	63.39
	O	29.17
	Al	6.44
CNT	C	96.48
	O	3.52
CNTAL10	C	68.96
	O	18.86
	Al	11.18
CNTAL5	C	86.53
	O	10.07
	Al	3.40
GO	C	79.07
	O	15.65
GOAL10	C	68.08
	O	23.80
	Al	9.12
GOAl5	C	69.40
	O	26.31
	Al	4.30

adsorbents which represent higher adsorption capacity for DBT molecules compared to unmodified adsorbents, the goodness of fit values (R^2; the squares of the correlation coefficients) of $\ln(q_e)$ versus $\ln(C_e)$ (for the linearized form of Freundlich equation) were comparable or slightly better than those of C_e/q_e versus C_e (for the linearized form of Langmuir's equation). This indicates complexity and non-uniformity of adsorbents and predominates of multilayer adsorption.

It was found that the maximum adsorption capacity Q_{max} for DBT on AC, ACAL10 and ACAL5 follows the trend ACAL5 > ACAL10 > AC. In a similar manner Q_{max} for CNT, CNTAL10 and CNTAL5 follows the trend CNTAL5 > CNTAL10 > CNT. On the other hand Q_{max} for GO, GOAL0 and GOAL5 follows the different trend GOAL5 > GO > GOA10. The Q_{max} values for AC, ACAL10 and ACAL5 are higher than those for CNT, CNTAL10 and CNTAL5 which are in turn higher than those for GO, GOAL10 and GOAL5. AC and CNT impregnated with 5% Al and 10.9% Al had, respectively Q_{max} values nearly double and 1.5 times those of their un-impregnated forms. Within the uncertainties in the Q_{max} values for GO, GOAL10 and GOAL5 it can be safely stated that there is no significant change in the Q_{max} value of GO after impregnation with either 5% Al or with 10.9% Al. This may be explained by agglomeration of the graphene oxide layers after their impregnation with Al in the form of Al_2O_3 which is confirmed by the SEM and TEM results. The highest adsorption capacity (85 ± *1* mg/g) was by ACAL5 and the others follow the order ACAL10 > AC > CNTAL5 > CNTAL10 > GOAL5 > CNT > GO > GOAL10. The increase in the adsorption of DBT from model diesel using carbon adsorbents loaded with Al_2O_3 is a consequence of the synergetic effect of introduction an additional acidic adsorption sites on the surface of carbon rather than an increase in the surface area and pore volume. In other words the unsaturated surface of amphoteric Al_2O_3 acts as a Bronsted acid and Lewis acid in the environment of the base DBT. The possible interaction between DBT molecules and carbon surface modified with Al_2O_3 adsorbent is illustrated in Fig. 8.

3.3. Adsorption kinetics of DBT

Studying the adsorption kinetics in the batch mode is essential to design the adsorption columns for further study and for industrial applications (Song and Ma, 2003). The results presented in Fig. 9 show that for all the adsorbents in this study, the adsorption rates of DBT reach equilibrium within 90 min.

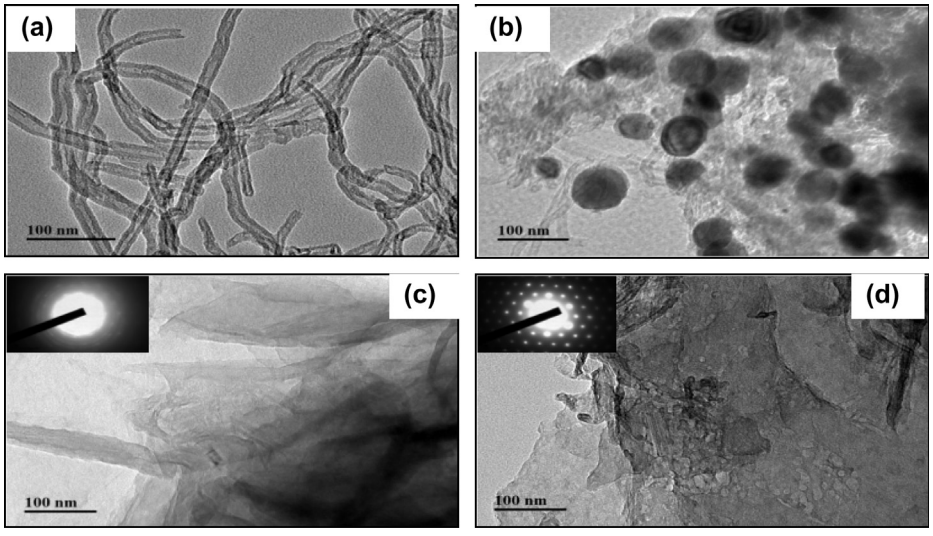

Figure 4 EF-TEM images for (a) CNT (b) GO before impregnation with Al_2O_3, (c) CNT and (d) GO after impregnation. The insets are diffraction patterns for the GO surface before and after impregnation with Al_2O_3.

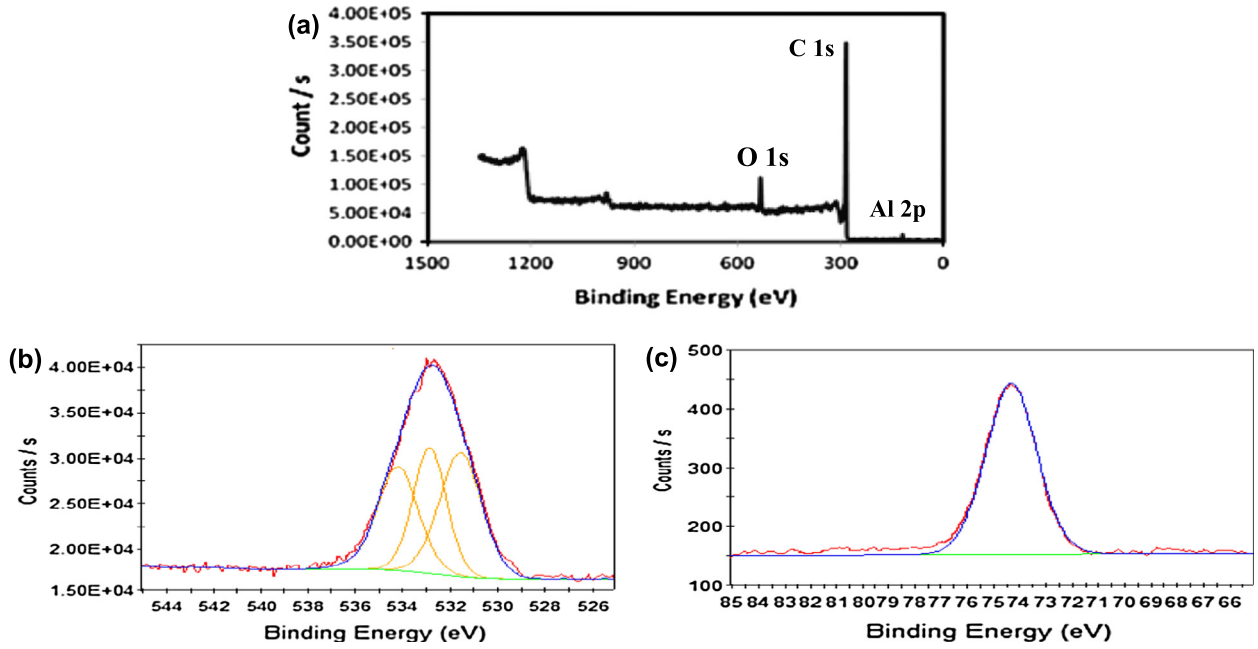

Figure 5 (a) XPS survey spectrum of CNT–Al_2O_3 (b) O 1s XPS spectrum of CNT–Al_2O_3 and (c) Al 2p XPS spectrum of CNT–Al_2O_3.

Table 3 Surface area, total pore volume and surface pH of AC, CNT and GO before and after their impregnation with 5% and 10.9% Al in the form of Al_2O_3.

Adsorbent	BET SA (m^2/g)	DFT V (cm^3/g)	pH
AC	882	0.45	9.4
ACAL10	799	0.41	8.9
ACAL5	825	0.39	8.5
CNT	217	1.51	5.8
CNTAL10	184	0.72	5.7
CNTAL5	118	0.55	5.5
GO	11	0.06	2.2
GOAL10	12	0.08	3.0
GOAL5	10	0.05	2.6

The experimental adsorption capacities ($q_{e,exp}$) for DBT on the carbonaceous adsorbents modified with aluminum oxide are given in Table 5. The initial fast adsorption is attributed to the large number of available active adsorption sites while the slowness at which maximum adsorption is reached is due to the few adsorption sites and the repulsive forces between adsorbate molecules in solution and adsorbate molecules on the adsorbents. The adsorption results were fitted using the kinetic models reported by Lagergren (1898) and Ho and McKay (1998) that led to Eqs. (9) and (10) for, respectively, a pseudo-first order adsorption rate,

$$\ln(q_e - q_t) = \ln(q_e) - k_1 t \tag{9}$$

and a pseudo-second order adsorption rate,

$$\frac{t}{q_t} = \frac{1}{q_e^2 k_2} + \frac{t}{q_e} \tag{10}$$

where q_e (mg/g) is the adsorption capacity at equilibrium, q_t in (mg/g) is the adsorption capacity at a time t (min), k_1 (min^{-1}) is the pseudo-first order rate constant and k_2 (g mg^{-1} min^{-1}) is the pseudo-second order rate constant. Linear least squares fits of $\ln(q_e - q_t)$ versus t for the adsorption data of DBT yielded low correlation coefficients (R) and are not reported. On the other hand linear least squares fits of $\frac{t}{q_t}$ versus t yielded correlation coefficients equal or very close to 1 and the experimental adsorption capacities ($q_{e,exp}$) values are very close to the predicted adsorption capacities ($q_{e\ pred}$) (see Table 5). Clearly the adsorption process follows pseudo second order kinetics. This indicates a chemical adsorption might be the rate determining step.

The mechanism of adsorption can be explored by studying the adsorption kinetics. Bearing in mind that the kinetic results fit perfectly into the pseudo second order kinetic model for DBT in all adsorbents, the influence of mass transfer resistance on their binding on the adsorbents was verified using Weber and Morris intra-particle diffusion model which allows exploring the intra-particle diffusion resistance using Eq. (11) (Weber, 1963):

$$q_e = k_{id} t^{0.5} + C \tag{11}$$

where k_{id} is the intra-particle diffusion rate constant (mg/g $min^{0.5}$), and C is a constant related to the thickness of the boundary layer (mg/g). Thus, the diffusion constant, k_{id}, can be obtained from the slope of the plot of q_t versus the square root of time. If this plot passes through the origin, then intra-particle diffusion is the rate controlling step.

Fig. 10 shows plots of q_t versus $t^{0.5}$ for DBT on ACAL10, CNTAL10 and GOAL10. These results imply that the adsorption processes involve more than a single kinetic stage or sorption rate (Weber, 1963). All adsorbents exhibited two stages, which can be attributed to two linear parts. The first linear part can be attributed to intra-particle diffusion, which produces a delay in the adsorption process. The second stage may be

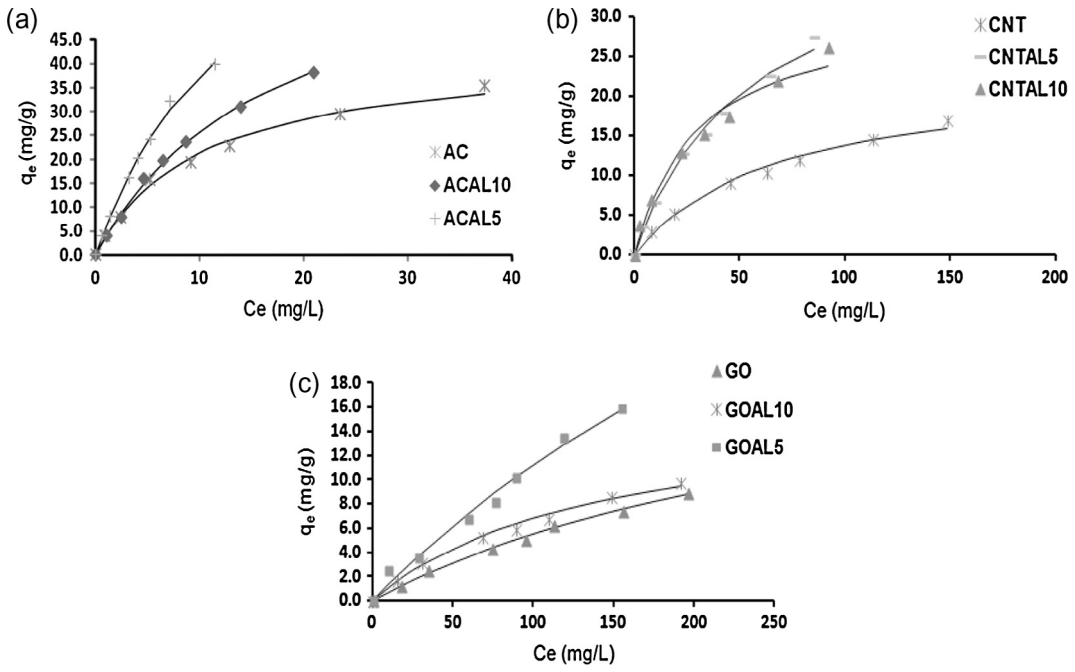

Figure 6 Adsorption isotherms at 25 °C for (a) DBT on AC, ACAL5 and ACAL10, (b) DBT on CNT, CNTAL5 and CNTAL10 and (c) DBT on GO, GOAL5 and GOAL10. Solid lines are fit to the Langmuir model.

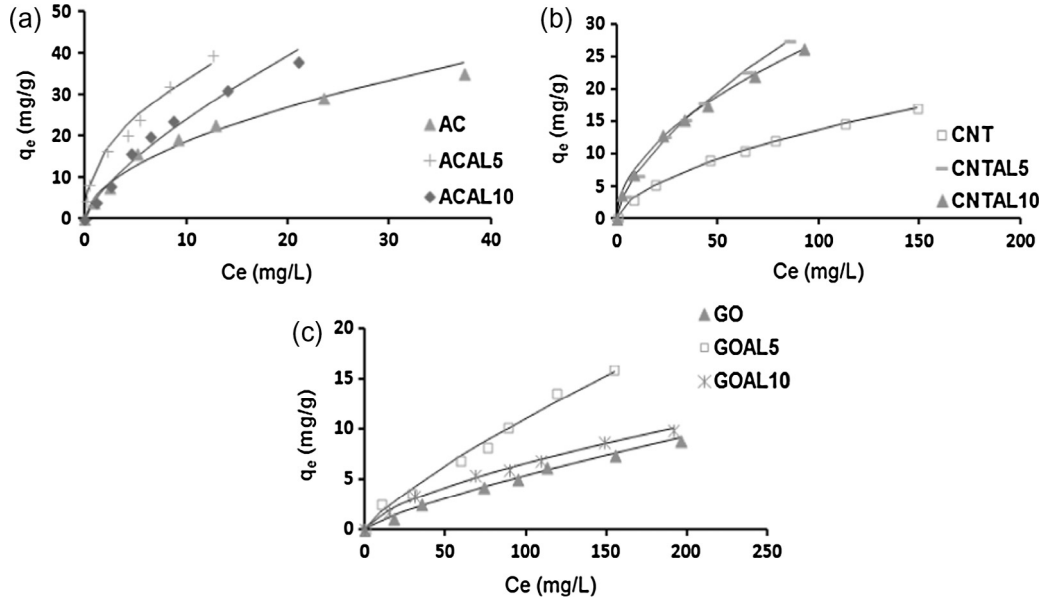

Figure 7 Adsorption isotherms at 25 °C for (a) DBT on AC, ACAL5 and ACAL10, (b) DBT on CNT, CNTAL5 and CNTAL10 and (c) DBT on GO, GOAL5 and GOAL10. Solid lines are fit to the Freundlich model.

regarded as the diffusion through smaller pores, which is followed by the establishment of equilibrium. The presence of micropores on the adsorbents is in line with this stage. Table 6 shows the calculated values of the diffusion constants for DBT on ACAL10, CNTAL10 and GOAL10. Higher values of k_{id} represent a faster net rate of adsorption as a result of slow desorption because of the improved bonding between DBT and the adsorbent.

3.4. Effect of adsorbent dosage

The results presented in Fig. 11 show that the percentage removal of DBT increased with the increase in the dose of AC loaded with Al_2O_3. High removal percentage of DBT (around 98%) was found at an adsorbent dosage of 500 mg for ACAL5 and ACAL10, while the maximum adsorption of

Table 4 Freundlich and Langmuir parameters and correlation coefficient for DBT adsorption on carbonaceous materials before and after doping with Al_2O_3.

Adsorbent	Freundlich			Langmuir		
	n [a]	K_F [b] ($mg^{(1-1/n)}$ mg^{-1} $L^{1/n}$)	R^2	Q_{max} [c] (mg/g)	b [d] (dm^3/mg)	R^2
AC	1.7 ± *0.1*	4.9 ± *0.5*	0.9747	42 ± *3*	(1.1 ± *0.1*) × 10^{-1}	0.9795
CNT	1.69 ± *0.04*	(8.9 ± *0.5*) × 10^{-1}	0.9968	24 ± *2*	(1.5 ± *0.1*) × 10^{-2}	0.9702
GO	1.22 ± *0.05*	(1.2 ± *0.2*) × 10^{-1}	0.9912	23 ± *3*	(3.0 ± *1.0*) × 10^{-3}	0.9201
ACAL10	1.29 ± *0.08*	4.94 ± *0.04*	0.9821	70 ± *3*	(4.7 ± *0.2*) × 10^{-2}	0.8503
ACAL5	1.26 ± *0.04*	6.3 ± *0.2*	0.9953	85 ± *1*	(7.8 ± *0.3*) × 10^{-2}	0.9603
CNTAL10	1.93 ± *0.04*	2.5 ± *0.1*	0.9982	33 ± *4*	(3.4 ± *0.2*) × 10^{-2}	0.9395
CNTAl5	1.55 ± *0.04*	1.6 ± *0.1*	0.9973	41 ± *4*	(2.10 ± *0.01*) × 10^{-2}	0.9450
GOAL10	1.49 ± *0.05*	(3.0 ± *0.3*) × 10^{-1}	0.9935	16 ± *2*	(7.3 ± *0.1*) × 10^{-3}	0.9571
GOAL5	1.4 ± *0.1*	(4 ± *1*) × 10^{-1}	0.9562	29 ± *9*	(6.1 ± *0.9*) × 10^{-3}	0.5310

[a] The uncertainty was calculated on the basis of the uncertainty in the slope of the Freundlich linearized equation.
[b] The uncertainty was calculated on the basis of the uncertainty in the intercept of the Freundlich linearized equation.
[c] The uncertainty was calculated on the basis of the uncertainty in the slope of the Langmuir linearized equation.
[d] The uncertainty was calculated on the basis of the uncertainty in the intercept of the Langmuir linearized equation.

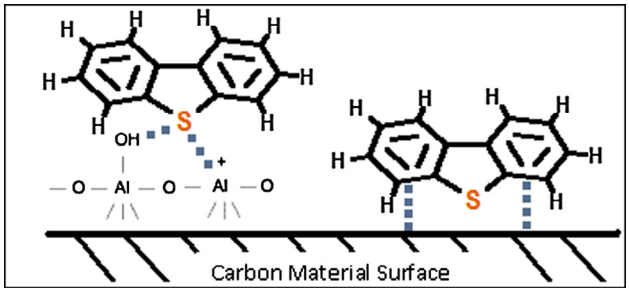

Figure 8 Possible interactions of DBT molecules with the developed adsorbents.

DBT (100% removal) was found at an adsorbent dosage of 1500 mg. 80% removal of DBT was obtained when CNTAL5 and CNTAL10 were used. Low removal of DBT was noticed when GO loaded with Al_2O_3 was used, due to its low surface area and fewer adsorption sites compared to the impregnated AC and CNT.

3.5. Selectivity of adsorption

The ACAL5 and CNTAL5 exhibit high adsorption capacities for DBT which are around 54 and 34 mg/g respectively. Using these adsorbents the removal efficiency was around 4 times the removal efficiency of naphthalene. However, the selectivity factors of DBT to naphthalene were 25 by ACAL5 and 7 by CNTAL5. On the other hand the selectivity factor of DBT to thiophene was around 255 using ACAL5 and 127 using CNTAL5. The selectivity factor of DBT to thiophene and naphthalene can be explained by three main factors. First, the size of the DBT molecule is closer to the size of the adsorbents' pores which allows them to be preferably trapped into the adsorbent. The second factor is the higher dipole moment, molar mass and aromaticity of DBT which lead to stronger van der Waals and π–π interactions with the adsorbents surface. The third factor is the higher basicity of DBT relative to thiophene and in turn its stronger acid–base interaction with the Al_2O_3 (Lewis acid) on the adsorbent surface.

3.6. Regeneration of adsorbents

Since the cost effectiveness and regeneration of the adsorbents are significant factors for actual diesel desulfurization their reusability has been considered. The regeneration procedure for ACAL5 and CNTAL5 was very simple. Upon the completion of adsorption experiments, the ACAL5 and CNTAL5 loaded with DBT were filtrated and then heated at 350 °C for 2 h in air to remove the adsorbed DBT molecules. The regenerated ACAL5 and CNTAL5 were reused for the next

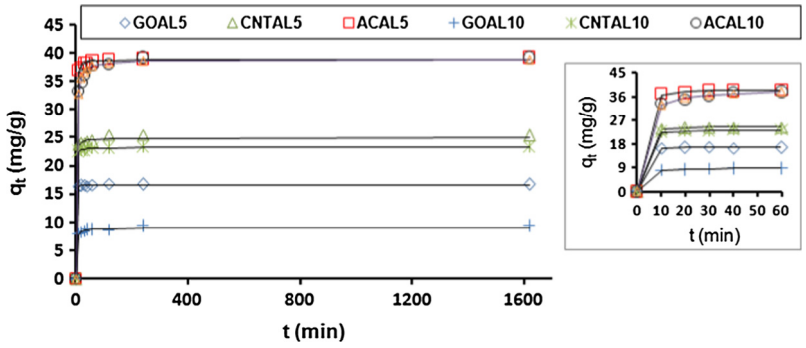

Figure 9 The effect of agitation time on the adsorption capacity of dibenzothiophene (DBT), using different adsorbents impregnated with different percentages of Al_2O_3. The insets show the effect of agitation time in the first 60 min.

Table 5 Pseudo-second order kinetic parameters for DBT adsorption on the carbonaceous materials loaded with Al_2O_3.

Adsorbent	Pseudo-second order parameters			
	DBT (250 mg/L)			
	$q_{e\ exp}$ (mg/g)	$q_{e\ pred.}$[a] (mg/g)	k_2[b] (g/mg min)	R^2
ACAL10	39.3	38.7 ± 0.2	0.015 ± 0.002	0.9999
CNTAL10	23.4	23.4 ± 0.1	0.09 ± 0.02	1.0000
GOAL10	9.4	9.5 ± 0.2	0.035 ± 0.02	0.9981
ACAL5	39.2	39.1 ± 0.1	0.033 ± 0.004	1.0000
CNTAL5	25.4	25.7 ± 0.3	0.02 ± 0.01	0.9993
GOAL5	16.8	16.8 ± 0.1	0.15 ± 0.07	0.9999

[a] The uncertainty was calculated from the uncertainty in the slope of the linearized equation.
[b] The uncertainty was calculated from the uncertainty in the intercept of the linearized equation.

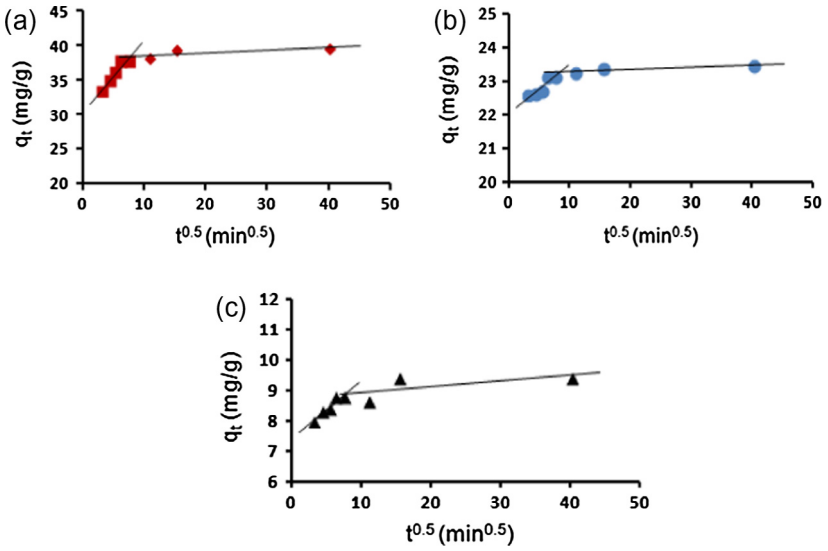

Figure 10 Plots of q_t versus $t^{0.5}$ showing the two diffusion stages predicted by the diffusion model for DBT adsorption on (a) ACAL10, (b) CNTAL10 and (c) GOAL10.

Table 6 Intra-particle diffusion parameters for DBT on different adsorbents.

Adsorbents	Intra-particle diffusion parameters		
	k_{id}	C	R^2
ACAL10	1.04	30.3	0.9338
CNTAL10	0.14	22.1	0.8046
GOAL10	0.19	7.4	0.9089

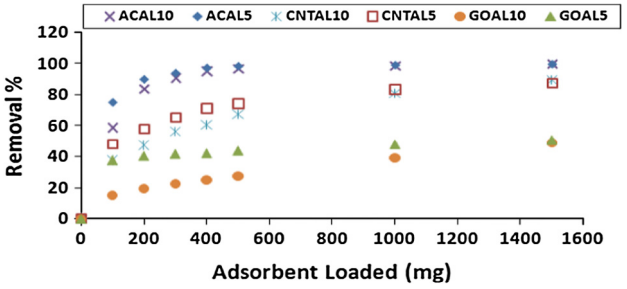

Figure 11 Effect of adsorbents loaded on the removal efficiency of dibenzothiophene (DBT) on AC, CNT and GO impregnated by Al_2O_3.

adsorption, and the successive adsorption–desorption cycles were repeated five times. As shown in Fig. 12, ACAL5 and CNTAL5 remained, within experimental error, nearly unchanged in their ability for DBT adsorption for at least five cycles.

As shown in Table 7, loaded AC and CNT with 5% Al in the form of Al_2O_3 adsorbents for removal of DBT sulfur compound with simple regeneration procedure and high selectivity have a comparable or slightly higher adsorption capacity than other reported adsorbents in the literature.

3.7. Adsorption of DBT from a real diesel sample

The potential application of using ACAL5 which has the best adsorption capacity and selectivity among the prepared adsorbents was evaluated for DBT removal from real diesel by measuring the DBT concentration before and after the adsorption based on the standard addition method. The original DBT was around 43 mg/L and was reduced by about 30%. Furthermore

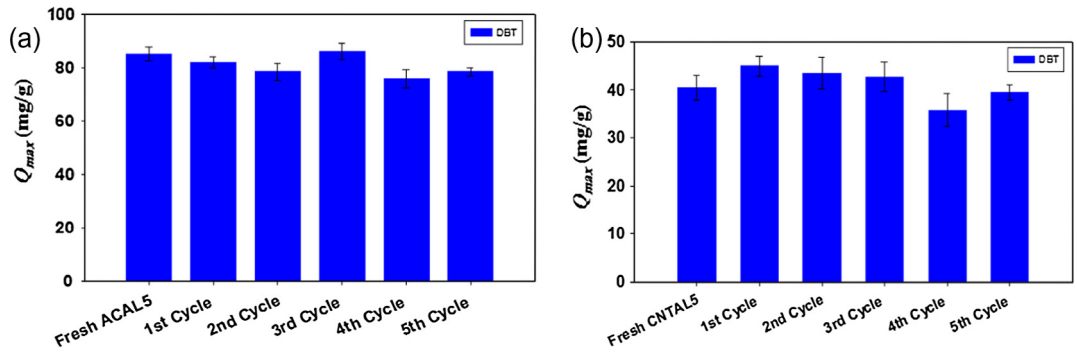

Figure 12 The adsorption capacities with error bars after each of 5 adsorbent regeneration cycles for (a) DBT on the ACAL5 adsorbent and (b) DBT on the CNTAL5 adsorbent.

Table 7 Adsorption capacity of DBT on different adsorbents from different model fuel media.

Adsorbent	Sulfur compound	Model diesel	Adsorption capacity (mg/g)	References
Alumina	DBT	*n*-Hexane	21.0	Srivastav and Srivastava (2009)
ACWS[a]	DBT	*n*-Heptane	47.1	Yang et al. (2007)
D-MIP/CMSs[b]	DBT	*n*-Hexane	105.0	Liu et al. (2014)
ACFH[c]	DBT	*n*-Hexane	14.0	Moosavi et al. (2012)
ACFH-Cu(I)[d]	DBT	*n*-Hexane	19.0	
Fe_3O_4@-SiO_2@MIPs[e]	DBT	*n*-Octane	63.3	Li et al. (2012)
Nanocrystalline NaY Zeolite	DBT	*n*-Nonane	1.7	Tang et al. (2011)
CP(m)/MIL100(Fe)[f]	DBT	*n*-Octane	110.0	Hasan and Jhung (2015)
ACAL5	DBT	*n*-Hexane	84.5 ± 0.8	This work
CNTAL5	DBT	*n*-Hexane	40.6 ± 4.4	This work

[a] Activated carbon treated with steam at 900 °C then washed by H_2SO_4.
[b] Carbon microsphere modified with double molecularly imprinted polymer.
[c] Activated carbon fiber thermally treated.
[d] Activated carbon fiber thermally treated and modified with copper cation.
[e] Iron oxide coated with silicon oxide nanoparticles coated with molecularly imprinted polymer.
[f] Cu(I)-containing compound/iron-benzenetricarboxylate $[Fe(III)_3O\text{-}(H_2O)_2(F)\{C_6H_3(CO_2)_3\}_2 \cdot nH_2O$ ($n \sim 14.5$).

to check the effectiveness of this adsorbent for DBT removal at higher concentration, a real diesel sample was spiked with DBT to increase its concentration in the original diesel sample to 153 mg/L. The adsorption results show that the DBT concentration was reduced to 102 mg/L with removal percentage about 33%. This relatively low removal efficiency is attributable to the severe medium of a real diesel which contains other competing aliphatic and aromatic sulfur compounds. In addition, the solubility of DBT in these components is much higher and its diffusion to the adsorbent surface is very low compared with its diffusion in the model diesel used in this study. Nevertheless this adsorbents proved its ability to remove about 30% of the DBT in real diesel.

4. Conclusion

Three different types of carbonaceous adsorbents namely AC, CNT and GO loaded with two loadings of Al (5% and 10.9%) in the form of Al_2O_3 were used for the removal of DBT from *n*-hexane as a simulant of diesel fuel. The Al_2O_3 was impregnated successfully on the surface of carbon materials using the wetness impregnation technique. The highest removal efficiency of DBT was achieved using the ACAL5 adsorbent. The adsorption capacities were 85 mg/g for DBT. The selectivity study of DBT relative to thiophene and DBT relative to naphthalene was carried out using ACAL5 and CNTAL5. It has been found that in ACAL5 the selectivity factor of DBT/thiophene was 255 and of DBT/naphthalene was 25, while in CNTAL5 the selectivity of DBT/thiophene was 127 and of DBT/naphthalene was 7. The results showed that modification of the AC, CNT and GO with Al_2O_3 resulted in enhancing the surface chemistry of adsorbents and in turn increase in their adsorption capacities and selectivity for DBT from model diesel. This is a consequence of introduction of additional acidic adsorption sites on the surface of carbon rather than an increase in the surface area and pore volume. These adsorbents showed good reusability for at least 5 adsorption cycles without significant loss in their adsorption capacity. It has also been found that ACAL5 is capable of removing 30% of the DBT in real diesel fuel.

Acknowledgment

The authors acknowledge the support for this research by the Chemistry Department and Center for Integrative Petroleum Research (CIPR) in the Research Institute (RI) at King Fahd University of Petroleum & Minerals (KFUPM).

Appendix A. Supplementary material

Supplementary data associated with this article can be found, in the online version, at http://dx.doi.org/10.1016/j.arabjc.2015.12.003.

References

Abu Safieh, K.A., Al-Degs, Y.S., Sunjuk, M.S., Saleh, A.I., Al-Ghouti, M.A., 2015. Selective removal of dibenzothiophene from commercial diesel using manganese dioxide-modified activated carbon: a kinetic study. Environ. Technol. 36, 98–105.

Adamson, A.W., Gast, A.P., 1967. Physical Chemistry of Surfaces.

Ahmad, W., Ahmad, I., Ishaq, M., Ihsan, K., 2017. Adsorptive desulfurization of kerosene and diesel oil by Zn impregnated montmorollonite clay. Arab. J. Chem. 10 (Suppl. 2), S3263–S3269.

Beardsley, M., Lindhjem, C., 1998. Exhaust Emission Factors for Nonroad Engine Modeling-Compression Ignition. United States Environmental Protection Agency (EPA), p. 11.

Bertelsen, B.I., 2001. The US motor vehicle emission control programme. Platin. Metals Rev. 45, 50–59.

Chamack, M., Mahjoub, A., Aghayan, H., 2014. Catalytic performance of vanadium-substituted molybdophosphoric acid supported on zirconium modified mesoporous silica in oxidative desulfurization. Chem. Eng. Res. Des.

Chen, H., Zhou, X., Shang, H., Liu, C., Qiu, J., Wei, F., 2004. Study of dibenzothiophene adsorption over carbon nanotube supported CoMo HDS catalysts. J. Nat. Gas Chem. 13, 209–217.

Commission, E.E., 2009. Directive 2009/30/EC of the European Parliament and of the Council of 23 April 2009 amending Directive 98/70/EC as regards the specification of petrol, diesel and gas–oil and introducing a mechanism to monitor and reduce greenhouse gas emissions and amending Council Directive 1999/32/EC as regards the specification of fuel used by inland waterway vessels and repealing Directive 93/12. EEC.

Cortes-Jácome, M., Morales, M., Angeles Chavez, C., Ramírez-Verduzco, L., López-Salinas, E., Toledo-Antonio, J., 2007. WO_x/TiO_2 catalysts via titania nanotubes for the oxidation of dibenzothiophene. Chem. Mater. 19, 6605–6614.

Directive, C., 1998. 98/70/EC of the European Parliament and of the Council of 13 October 1998 Relating to the Quality of Petrol and Diesel Fuels and Amending Council Directive 93/12. EEC.

Dubinin, M., 1966. Porous structure and adsorption properties of active carbons. Chem. Phys. Carbon 2, 51–120.

Gutiérrez-Alejandre, A., Larrubia, M.A., Ramirez, J., Busca, G., 2006. FT-IR evidence of the interaction of benzothiophene with the hydroxyl groups of H-MFI and H-MOR zeolites. Vib. Spectrosc. 41, 42–47.

Hasan, Z., Jhung, S.H., 2015. A facile method to disperse non-porous metal organic frameworks: composite formation with a porous metal organic framework and application in adsorptive desulfurization. ACS Appl. Mater. Interfaces.

Ho, Y., McKay, G., 1998. A comparison of chemisorption kinetic models applied to pollutant removal on various sorbents. Process Saf. Environ. Protect. 76, 332–340.

Hummers Jr., W.S., Offeman, R.E., 1958. Preparation of graphitic oxide. J. Am. Chem. Soc. 80, 1339.

Ishaq, M., Sultan, S., Ahmad, I., Ullah, H., Yaseen, M., Amir, A., 2015. Adsorptive desulfurization of model oil using untreated, acid activated and magnetite nanoparticle loaded bentonite as adsorbent. J. Saudi Chem. Soc.

Kim, J.H., Ma, X., Zhou, A., Song, C., 2006. Ultra-deep desulfurization and denitrogenation of diesel fuel by selective adsorption over three different adsorbents: a study on adsorptive selectivity and mechanism. Catal. Today 111, 74–83.

Kumagai, S., Ishizawa, H., Toida, Y., 2010. Influence of solvent type on dibenzothiophene adsorption onto activated carbon fiber and granular coconut-shell activated carbon. Fuel 89, 365–371.

Lagergren, S., 1898. About the theory of so-called adsorption of soluble substances. Kungliga Svenska Vetenskapsakademiens Handlingar 24, 1–39.

Lastoskie, C., Gubbins, K.E., Quirke, N., 1993. Pore size distribution analysis of microporous carbons: a density functional theory approach. J. Phys. Chem. 97, 4786–4796.

Li, H., Xu, W., Wang, N., Ma, X., Niu, D., Jiang, B., Liu, L., Huang, W., Yang, W., Zhou, Z., 2012. Synthesis of magnetic molecularly imprinted polymer particles for selective adsorption and separation of dibenzothiophene. Microchim. Acta 179, 123–130.

Li, L., Quinlivan, P.A., Knappe, D.R., 2002. Effects of activated carbon surface chemistry and pore structure on the adsorption of organic contaminants from aqueous solution. Carbon 40, 2085–2100.

Liu, W., Liu, X., Yang, Y., Zhang, Y., Xu, B., 2014. Selective removal of benzothiophene and dibenzothiophene from gasoline using double-template molecularly imprinted polymers on the surface of carbon microspheres. Fuel 117, 184–190.

Liu, Y., She, N., Zhao, J., Peng, T., Liu, C., 2013. Fabrication of hierarchical porous ZnO and its performance in Ni/ZnO reactive-adsorption desulfurization. Petrol. Sci. 10, 589–595.

Lucas, E., Decker, S., Khaleel, A., Seitz, A., Fultz, S., Ponce, A., Li, W., Carnes, C., Klabunde, K.J., 2001. Nanocrystalline metal oxides as unique chemical reagents/sorbents. Chem.-A Eur. J. 7, 2505–2510.

Mabayoje, O., Seredych, M., Bandosz, T.J., 2012. Enhanced reactive adsorption of hydrogen sulfide on the composites of graphene/-graphite oxide with copper (hydr) oxychlorides. ACS Appl. Mater. Interfaces 4, 3316–3324.

Matsuzawa, S., Tanaka, J., Sato, S., Ibusuki, T., 2002. Photocatalytic oxidation of dibenzothiophenes in acetonitrile using TiO_2: effect of hydrogen peroxide and ultrasound irradiation. J. Photochem. Photobiol. A: Chem. 149, 183–189.

Moosavi, E.S., Dastgheib, S.A., Karimzadeh, R., 2012. Adsorption of thiophenic compounds from model diesel fuel using copper and nickel impregnated activated carbons. Energies 5, 4233–4250.

NIST XPS Database, 2015. Spectrum Search. <http://srdata.nist.gov/xps/EnergyTypeValSrch.aspx> (Last accessed on January of 2015).

Seredych, M., Bandosz, T.J., 2009. Selective adsorption of dibenzothiophenes on activated carbons with Ag Co, and Ni species deposited on their surfaces. Energy Fuels 23, 3737–3744.

Seredych, M., Bandosz, T.J., 2010a. Adsorption of dibenzothiophenes on activated carbons with copper and iron deposited on their surfaces. Fuel Process. Technol. 91, 693–701.

Seredych, M., Bandosz, T.J., 2010b. Adsorption of dibenzothiophenes on nanoporous carbons: identification of specific adsorption sites governing capacity and selectivity†. Energy Fuels 24, 3352–3360.

Seredych, M., Bandosz, T.J., 2011. Investigation of the enhancing effects of sulfur and/or oxygen functional groups of nanoporous carbons on adsorption of dibenzothiophenes. Carbon 49, 1216–1224.

Seredych, M., Lison, J., Jans, U., Bandosz, T.J., 2009. Textural and chemical factors affecting adsorption capacity of activated carbon in highly efficient desulfurization of diesel fuel. Carbon 47, 2491–2500.

Seredych, M., Wu, C.T., Brender, P., Ania, C.O., Vix-Guterl, C., Bandosz, T.J., 2012. Role of phosphorus in carbon matrix in desulfurization of diesel fuel using adsorption process. Fuel 92, 318–326.

Shi, Y., Zhang, X., Wang, L., Liu, G., 2014. MOF-derived porous carbon for adsorptive desulfurization. AIChE J. 60, 2747–2751.

Shiraishi, Y., Hara, H., Hirai, T., Komasawa, I., 1999. A deep desulfurization process for light oil by photosensitized oxidation using a triplet photosensitizer and hydrogen peroxide in an oil/

water two-phase liquid–liquid extraction system. Ind. Eng. Chem. Res. 38, 1589–1595.

Song, C., Ma, X., 2003. New design approaches to ultra-clean diesel fuels by deep desulfurization and deep dearomatization. Appl. Catal. B: Environ. 41, 207–238.

Song, H.S., Ko, C.H., Ahn, W., Kim, B.J., Croiset, E., Chen, Z., Nam, S.C., 2012. Selective dibenzothiophene adsorption on graphene prepared using different methods. Ind. Eng. Chem. Res. 51, 10259–10264.

Srivastav, A., Srivastava, V.C., 2009. Adsorptive desulfurization by activated alumina. J. Hazard. Mater. 170, 1133–1140.

Tanabe, K., 1981. Solid acid and base catalysts. Catal. Sci. Technol. 2, 255.

Tang, K., Hong, X., Zhao, Y., Wang, Y., 2011. Adsorption desulfurization on a nanocrystalline NaY zeolite synthesized using carbon nanotube templated growth. Petrol. Sci. Technol. 29, 779–787.

Tao, H., Nakazato, T., Sato, S., 2009. Energy-efficient ultra-deep desulfurization of kerosene based on selective photooxidation and adsorption. Fuel 88, 1961–1969.

Wang, L., Zhu, D., Duan, L., Chen, W., 2010. Adsorption of single-ringed N-and S-heterocyclic aromatics on carbon nanotubes. Carbon 48, 3906–3915.

Weber, W., Asce Jr., J.M., Morris, J.C., 1963. Kinetic of adsorption on carbon from solutions. J. Sanitary Eng. Div., Proc. Am. Soc. Civ. Eng., 31–59

Yang, R.T., Hernández-Maldonado, A.J., Yang, F.H., 2003. Desulfurization of transportation fuels with zeolites under ambient conditions. Science 301, 79–81.

Yang, S.-T., Chang, Y., Wang, H., Liu, G., Chen, S., Wang, Y., Liu, Y., Cao, A., 2010. Folding/aggregation of graphene oxide and its application in Cu^{2+} removal. J. Colloid Interface Sci. 351, 122–127.

Yang, Y., Lu, H., Ying, P., Jiang, Z., Li, C., 2007. Selective dibenzothiophene adsorption on modified activated carbons. Carbon 45, 3042–3044.

Yu, G., Lu, S., Chen, H., Zhu, Z., 2005. Diesel fuel desulfurization with hydrogen peroxide promoted by formic acid and catalyzed by activated carbon. Carbon 43, 2285–2294.

Zhou, A., Ma, X., Song, C., 2006. Liquid-phase adsorption of multi-ring thiophenic sulfur compounds on carbon materials with different surface properties. J. Phys. Chem. B 110, 4699–4707.

Zhu, W., Li, H., Jiang, X., Yan, Y., Lu, J., Xia, J., 2007. Oxidative desulfurization of fuels catalyzed by peroxotungsten and peroxomolybdenum complexes in ionic liquids. Energy Fuels 21, 2514–2516.